Manuscript Title:	Structure and Dynamics of Single-isoform Recombinant Neuronal Human Tubulin
Manuscript No:	JBC/2016/731133 [R1]
Manuscript Type:	Report
Date Submitted by the Author:	19 Apr 2016
Complete List of Authors:	Annapurna Vemu, Joseph Atherton, Jeffrey O. Spector, Agnieszka Szyk, Carolyn A. Moores, and Antonina Roll-Mecak
Keywords:	cryo-electron microscopy; cytoskeleton; microscopy; microtubule; tubulin ; dynamic instability; engineered tubulin; microtubule dynamics ; recombinant tubulin; tubulin isoform

Structure and Dynamics of Single-isoform Recombinant Neuronal Human Tubulin

Annapurna Vemu[1§], Joseph Atherton[2§], Jeffrey O. Spector[1§], Agnieszka Szyk[1], Carolyn A. Moores[2,*] and Antonina Roll-Mecak[1,3,*]

[1] Cell Biology and Biophysics Unit, National Institute of Neurological Disorders and Stroke, Bethesda, MD 20892, U.S.A.
[2] Institute of Structural and Molecular Biology, Department of Biological Sciences, Birkbeck College, University of London, London, United Kingdom
[3] Biophysics Center, National Heart, Lung and Blood Institute, Bethesda, MD 20892, U.S.A.
[§] these authors contributed equally

[*] Correspondence should be addressed to: Carolyn Moores, Institute of Structural and Molecular Biology, Birkbeck College, London, United Kingdom Telephone: 020 7631 6858; Email: c.moores@mail.cryst.bbk.ac.uk and Antonina Roll-Mecak, Cell Biology and Biophysics Unit, Porter Neuroscience Research, Center National Institutes of Health, Building 35, Room 3B-203,35 Convent Drive, MSC 3700, Bethesda, MD 20892-3700, Telephone: 301-814-8119, Email: Antonina@mail.nih.gov

Running title: *Structure and dynamics of recombinant human α1A/βIII tubulin*

Keywords: microtubule dynamics, tubulin, engineered tubulin, recombinant tubulin, tubulin isoform, microtubule structure, cryo-EM, posttranslational modification,

Microtubules are polymers that cycle stochastically between polymerization and depolymerization i.e., they exhibit "dynamic instability". This behavior is crucial for cell division, motility and differentiation. While studies in the last decade have made fundamental breakthroughs in our understanding of how cellular effectors modulate microtubule dynamics, analysis of the relationship between tubulin sequence, structure and dynamics has been held back by a lack of dynamics measurements with and structural characterization of homogenous, isotypically pure, engineered tubulin. Here we report for the first time the cryo-EM structure and *in vitro* dynamics parameters of recombinant isotypically pure human tubulin. α1A/βIII is a purely neuronal tubulin isoform. The 4.2 Å structure of unmodified human α1A/βIII microtubules shows overall similarity to that of heterogeneous brain microtubules, but is distinguished by subtle differences at polymerization interfaces, which are hotspots for sequence divergence between tubulin isoforms. *In vitro* dynamics assays show that, like mosaic brain microtubules, recombinant homogenous microtubules undergo dynamic instability but they polymerize slower and catastrophe less frequently. Interestingly, we find that epitaxial growth of α1A/βIII microtubules from heterogeneous brain seeds is inefficient, but can be fully rescued by incorporating as little as 5% of brain tubulin into the homogenous α1A/βIII lattice. Our study establishes a system to examine the structure and dynamics of mammalian microtubules with well-defined tubulin species and is a first and necessary step towards uncovering how tubulin genetic and chemical diversity is exploited to modulate intrinsic microtubule dynamics.

Microtubules cycle stochastically between periods of polymerization and depolymerization; *i.e.*, they exhibit "dynamic instability" (1). This behavior is crucial in cell division, motility and differentiation. Despite the discovery of dynamic instability more than thirty years ago (1) and fundamental breakthroughs in our understanding of microtubule dynamics modulation by cellular effectors (2,3), analysis of the relationship between tubulin sequence, structure and dynamics

has been held back by a lack of structural and *in vitro* dynamics data with homogenous, isotypically pure, engineered tubulin. Eukaryotes have multiple tubulin genes (humans have eight α and eight β-tubulin isotypes) with tissue specific distributions (4). Some microtubules are isotype mixtures, while others are formed from a predominant single isotype (5). Moreover, tubulin is subject to abundant and chemically diverse posttranslational modifications that include acetylation, detyrosination, phosphorylation, glutamylation, glycylation and amination (6,7). Virtually all biochemical studies have used tubulin purified from mammalian brain tissue through multiple cycles of *in vitro* depolymerization and polymerization (8). While tubulin is abundant in this source, the resulting material is highly heterogeneous, being comprised of multiple tubulin isotypes bearing chemically diverse and abundant posttranslational modifications (9-11). More than twenty-two different charge variants are repolymerized in random fashion for *in vitro* polymerization assays (12). Thus, microtubules used for *in vitro* dynamics assays have been mosaic, with random distributions of isoforms and posttranslational modifications. Moreover, this purification procedure selects tubulin subpopulations that polymerize robustly while discarding those that do not. Efforts to reduce metazoan tubulin heterogeneity exploited differences in isoform compositions between various tissues or cell lines (e.g. avian erythroctyes (13) and HeLa cells (14)) or the use of isoform specific antibodies for immunopurification (15). However, neither of these approaches yielded homogenous, single-isoform tubulin. Here we report for the first time the expression and purification of recombinant isotypically pure unmodified human tubulin competent for *in vitro* dynamics assays and report its dynamic parameters as well as cryo-EM structure at 4.2 Å resolution. We find that isotypically pure unmodified α1A/βIII tubulin exhibits subtle differences in dynamics when compared with heterogeneous brain tubulin, consistent with the small conformational rearrangements at tubulin polymerization interfaces revealed by our near-atomic resolution structure of α1A/βIII microtubules. Our study establishes a system to examine the structure and dynamics of mammalian microtubules with well-defined α and β-tubulin species and is a first and necessary step towards exploring the biophysical correlates between sequence, structure and dynamics for mammalian microtubules.

EXPERIMENTAL PROCEDURES

Expression and Purification of Human Recombinant Tubulin Constructs - Codon optimized genes for human α1A tubulin (NP_001257328) with an internal His-tag in the acetylation loop and a Prescission protease cleavable C-terminally flag-tagged βIII tubulin (NM_006077) were custom synthesized by Integrated DNA Technologies and cloned into a pFastBac™-Dual vector as described (16, 17). The internal His-tag in α-tubulin allowed production of an α-tubulin ending in its natural carboxy-terminal tyrosine (17,18). Without an affinity based selection for α-tubulin, the final sample contains ~30% contamination with endogenous insect α-tubulin species that can be variable from construct to construct. The Bac-to-Bac System (Life Technologies) was used to generate bacmids for baculovirus protein expression. HighFive or SF9 cells were grown to a density between 1.3-1.6 x10^6 cells/ml and infected with viruses at the multiplicity of infection of 1. Cultures were grown in suspension for 48 hours and cell pellets were collected, washed in PBS and flash frozen. Cells were lysed by gentle sonication in 1XBRB80 buffer (80 mM PIPES pH 6.9, 1 mM $MgCl_2$, 1mM EGTA) with addition of: 0.5 mM ATP, 0.5 mM GTP, 1mM PMSF and 25U/ml benzonase nuclease. The lysate was supplemented with 500 mM KCl and cleared by centrifugation (15 min at 400,000xg). The crude supernatant (supplemented with 25 mM Imidazole pH 8.0) was loaded on a Ni-NTA column (Qiagen) equilibrated with high salt buffer (BRB80, 500 mM KCl, 25 mM Imidazole). His-tagged tubulin was eluted with 250 mM Imidazole in BRB80 buffer. The eluate was further purified on anti-flag G1 affinity resin (Gen Script). Flag-tagged tubulin was eluted by incubation with flag peptide (Gen Script) at 0.25 g/L concentration followed by removal of the tag by Prescission protease. A final purification step was performed on a Resource Q anion exchange column (GE Healthcare) with a linear gradient from 100 mM to 1M KCl in BRB80 buffer. Peak

fractions were pooled and buffer exchanged on a PD10 desalting column (GE Healthcare) equilibrated with BRB80, 20 μM GTP. Small aliquots of tubulin were frozen in liquid nitrogen and stored at −80 °C until use. The purified tubulin was subjected to ESI-TOF LC-MS analysis and detected no endogenous tubulin or posttranslational modifications (Fig.1A). The sensitivity of our mass spectrometric analyses is high enough to detect as little as 1% contaminating posttranslationally modified tubulin species (17). The final yield is ~1 mg of 99% recombinant isotypically pure αβ-tubulin per L of SF9 cells.

Cryo-EM Sample Preparation and Data Collection - Recombinant human α1A/βIII tubulin was polymerized at a final concentration of 2.5mg/ml in BRB80 buffer (80mM PIPES, 2mM $MgCl_2$, 1mM EGTA, 1mM DTT) with 1mM GMPCPP or 2mM GTP at 37°C for 1 hour. GMPCPP-bound microtubules were double-cycled by depolymerizing on ice then repolymerized at 37°C for 1 hour with an additional 2mM GMPCPP. Stabilized α1A/βIII microtubules were diluted in BRB20 (20mM PIPES, 2mM $MgCl_2$, 1mM EGTA, 1mM DTT) to a final concentration of 2.5μM. Human kinesin-3 motor domain (Kif1A, residues 1-361 (19) was diluted to 20μM in BRB20 with 2mM AMPPNP. The microtubules and motor were applied sequentially to glow-discharged C-flat™ holey carbon grids (Protochips) and the sample was vitrified using a Vitrobot (FEI Co.). The presence of kinesin motor domain allowed differentiation between α- and β-tubulin during processing. Images were collected with a DE20 direct electron detector (Direct Electron) on a FEI Tecnai G2 Polara operating at 300kV with a calibrated magnification of 52,117x corresponding to a final sampling of 1.22Å/pixel. A total electron dose of ~50e-/$Å^2$ over a 1.5 seconds exposure and a frame rate of 15 frames/second was used, giving a total of 23 frames at ~2.2e-/frame. Dynamic microtubules grown from GMPCPP seeds were polymerized at 2mg/ml for 30 minutes, kept at 37°C throughout and vitrified as above. Images were collected on a FEI Tecnai T12 operating at 120kV using a 4kx4k CCD camera (Gatan Inc.).

Data Processing for 3D Reconstruction - Individual ~2.2e- frames were globally aligned using IMOD scripts (20) then locally aligned using the Optical Flow approach (21) implemented in Xmipp (22). The full dose of ~50e- was used for particle picking and CTF determination in CTFFind3 (23), whereas ~25e- was used in particle processing to center particles and determine their Euler angles. Euler angles and shifts determined using ~25e- dose were used to generate reconstructions from either the first ~25e- or ~12e- of the exposure. Kinesin-3 microtubules were manually boxed in Eman Boxer (24), serving as input for a set of custom-designed semi-automated single-particle processing scripts utilizing Spider and Frealign as described previously (25) with minor modifications. 10,164 particles or 142,296 asymmetric units were used in the final reconstruction, which was assessed for over-fitting using a high-resolution noise-substitution test (26). Using local resolution estimates determined with the *blocres* program in Bsoft, the reconstruction was sharpened with a B factor of -180 up to a resolution of 5.5Å or 4Å for visualization of kinesin or tubulin densities, respectively. The overall resolution of the reconstruction is 4.2Å (FSCtrue, 0.143 criteria) (26) encompassing a resolution range of ~3.5-5.5Å. The best regions of the reconstruction are within the tubulin portion of the complex (Fig. 1B and 2) from which we built an α1A/βIII microtubule model. The quality of our reconstruction was sufficient to confirm that GMPCPP was found in the E-site (Fig. 1C) and GTP in the N-site.

Model Building and Refinement - The polypeptide model of the unmodified α1A/βIII tubulin GMPCPP microtubule was built directly into density in Coot (27) using PDB 3JAT (28) as a starting model. The structure was refined under symmetry restraints in REFMAC v5.8 (29). Secondary structure and reference restraints based on the high-resolution tubulin crystal structure PDB 4DRX (30) were generated with ProSMART (31). Model building in Coot and refinement in REFMAC were repeated iteratively until the quality of the model and fit were optimized (Supplemental Table 1).

In vitro Microtubule Dynamics Assays - GMPCPP stabilized seeds were prepared as described (32). The GMPCPP seeds were immobilized in flow

chambers using neutravidin as previously described (33). The final imaging buffer contained 1XBRB80 supplemented with 1mM GTP, 100mM KCl, 1% pluronic F-127 and oxygen scavengers prepared as described (34). An objective heater (Bioptechs) was used to warm the chamber to 30°C. All chambers were sealed and allowed to equilibrate on the microscope stage for 5 minutes prior to imaging. Darkfield images were acquired every 5 seconds for 30 minutes. For depolymerization rate measurements the frame rate used was 40 fps. Imaging was performed on a Nikon Eclipse Ti-E equipped with a high NA darkfield condenser, a 100x adjustable iris objective and a Hamamatsu Flash4.0 v2 camera with 2x2 binning. The final pixel size was 108 nm. Darkfield illumination was provided by a Lumencor SOLA SE-II light engine. A Nikon GIF filter was used to protect the seeds from excessive photodamage. All solutions were filtered through a 0.1 μm filter.

Dynamic Parameter Measurements - Using ImageJ, kymographs were generated from dark-field images. Kymographs were traced by hand and dynamic parameters were calculated. Growth and depolymerization rates were determined from the slope of the growing or depolymerizing microtubule in the kymographs. Catastrophe frequency was determined as the number of observed catastrophes divided by the total time spent in the growth phase. Extremely rare rescue events were observed under our experimental conditions and thus were not quantified. Mean microtubule lifetime was calculated as the average time a microtubule spent in the growth phase before a catastrophe. Mean microtubule length was calculated as the average length a microtubule reached before a catastrophe. The probability of nucleation was determined by determining the percentage of seeds that nucleated in 30 minutes in a field of view. Dynamicity was determined as defined in Toso *et al* as the sum of total growth and shortening lengths divided by total time (35).

RESULTS

Near-atomic Resolution Structure of Single-isoform Human α1A/βIII Microtubules - We selected for our study α1A/βIII tubulin. βIII is a neuronal isoform that constitutes 25% of purified brain tubulin (10). It is expressed in non-neuronal tissues only during tumorigenesis (36,37). It is also the most divergent of all β-tubulin isotypes. It is highly overexpressed in non-neuronal cells upon transformation and has been identified as a strong prognosticator of poor clinical outcomes (37). We expressed human α1A/βIII tubulin in insect cells (16). Through a new double-selection strategy using affinity-tags on both α- and β-tubulin, we produced, for the first time, >99% homogenous, modification-free, single-isotype human αβ-tubulin, free of contamination from endogenous insect tubulins (Fig. 1A and see "Experimental Procedures") that is assembly-competent in the absence of stabilizing drugs like taxol and thus suitable for *in vitro* dynamics assays. Our tagging scheme generates an α-tubulin with a native carboxy-terminus and thus this recombinant tubulin is suitable for the investigation of the effects of the tubulin detyrosination/tyrosination cycle on intrinsic microtubule dynamics and those mediated by the modification dependent recruitment of cellular effectors (38,39).

To gain insight into the assembly properties of α1A/βIII recombinant tubulin we determined the structure of α1A/βIII microtubules in complex with the GTP analog GMPCPP at near-atomic resolution using cryo-electron microscopy and single-particle image reconstruction (25) (Figs. 1B and 2). There is a resolution gradient in the reconstruction, with the best resolution (~3.5Å) within the body of the microtubule (encompassing a resolution range of ~3.5-4.5Å, Fig. 2A). The resolution range of the kinesin motor domain, used to facilitate reconstruction is ~4.5-5.5Å. Overall, the reconstruction has a resolution of 4.2 Å (Fourier shell correlation, 0.143 criterion (26), encompassing a resolution range of ~3.5-5.5Å) (Figs. 2B, C). The reconstruction shows clearly resolved β-sheets and α-helical pitch (Figs. 2D, E and F). The majority (92%) of human α1A/βIII GMPCPP microtubules have 14 protofilaments, similar to brain GMPCPP microtubules (40). The tubulin monomer consists of a well-folded globular core and highly negatively charged and flexible C-terminal tails (41). The C-terminal tails are the locus of the greatest chemical heterogeneity in tubulin. They appear disordered in all microtubule structures to date either because (i) they have no unique well-defined conformation

or (ii) defined conformations unique to particular isoforms or posttranslationally modified forms are lost during the iterative averaging used in EM reconstructions due to the high heterogeneity of these tails in brain tubulin samples. Despite the chemical homogeneity of our sample, there is no density attributable to them, indicating that they are intrinsically disordered unless engaged by an effector as seen for the tubulin tyrosine ligase like 7 glutamylase or the NDC80 complex(42-44).

Consistent with the high sequence conservation of the tubulin body, our structure is similar to that of heterogenous mosaic mammalian brain GMPCPP microtubules and the overall conformation of the tubulin dimers in our reconstruction is consistent with a GTP-like extended conformation (28) (Fig. 1C). The backbone root-mean-square deviation (r.m.s.d) of our tubulin dimer model overlaid on that of the recently published structure of mammalian heterogenous brain GMPCPP 14 protofilament microtubules is <2Å. A difference in the tubulin repeat distance is observed between α1A/βIII and brain microtubules: 82.7 ± 0.2 v*s.* 83.1Å ± 0.0 measured from the EM reconstruction (i.e., model-independent); 82.6 *vs.* 83.2Å measured by comparing models, for α1A/βIII and brain microtubules, respectively (28,45). However, the tubulin repeat distance for the recombinant α1A/βIII microtubules (~82.7 Å) is roughly comparable with the repeat distance for heterogeneous brain GMPCPP microtubules (~83Å), which is more extended than that of the GDP state (~81.5Å)(28,45). Nevertheless, we find two subtle differences that have the potential to impact polymerization dynamics. First, the loop connecting helices H1 and H1' in β-tubulin shifts ~3Å away from the H1'-S2 loop, which makes lateral contacts with the M-loop (microtubule loop) of the neighboring dimer (Figs. 1D and E). The M-loop is a sequence element crucial to lateral contacts between adjacent protofilaments. Strikingly, the H1'-S2, H2-S3 and M-loops are a hotspot of sequence variation across β-tubulin isoforms (Fig. 1F), consistent with the structural plasticity we observe at this interface. Second, when one α protomer each of brain GMPCPP and recombinant α1A/βIII GMPCPP microtubule protofilaments are superimposed, a clear displacement of successive recombinant α1A/βIII dimers becomes apparent (Fig. 3A). This propagates from the exchangeable GTP-site (E-site) and βIII-tubulin longitudinal interface and results in a progressive stagger that increases with each dimer along the protofilament, such that the first neighboring dimer is offset by 1.7 Å (all Cα r.m.s.d.), the second by 3.4 Å and so on. Together, these relatively subtle structural differences could contribute to differences in dynamic properties. Interestingly, we find that at 6 μM α1A/βIII tubulin, 92% of α1A/βIII GMPCPP seeds nucleate microtubules but only 33% brain seeds nucleate α1A/βIII microtubules (Fig. 3B), suggestive of lattice mismatch effects between the brain microtubule seed and the lattice parameters of the growing α1A/βIII microtubule. This is consistent with the subtle structural differences between α1A/βIII and heterogeneous brain microtubules that we identified (Figs. 1D, 1E and 3A). Unexpectedly, robust growth off brain seeds at 6 μM α1A/βIII could be rescued (from 33% to 91%) if as little as 5% brain tubulin was added (Fig. 3B). Thus, a small level of tubulin heterogeneity can alleviate the nucleation defect that arises from the potential mismatch between the lattices of the two microtubule types. Our finding has intriguing consequences for the nucleation *in vivo* of microtubules composed of mixtures of tubulin isoforms.

In Vitro Dynamics of Single-isoform α1A/βIII Tubulin - To determine dynamic parameters of single-isoform α1A/βIII tubulin, we performed label-free *in vitro* dynamic assays using darkfield microscopy (46) (Fig. 4, supplemental Movies 1 and 2) so that our dynamic parameters are not confounded by effects arising from the addition of fluorescently labeled brain tubulin to the otherwise homogeneous microtubules. The α1A/βIII microtubules have the typical end-appearance observed for brain microtubules consisting of a mixture of short sheet-like and blunter structures (Fig. 4B) (47). To quantify their dynamics, we generated kymographs from time-lapse imaging of dynamic microtubule assays (Fig. 4*C*). The growth rates at the plus-end are 35% slower when compared with those of heterogenous brain tubulin while minus-end growth rates are statistically indistinguishable. Consistent with this, the on rate of α1A/βIII tubulin at the plus-end is 1.8 dimers s^{-}

^{1} μM^{-1} compared to the 3.6 dimers s^{-1} μM^{-1} for brain tubulin (our measurements for brain microtubules are similar to those reported in (48)). Darkfield imaging allows data collection at the high frame rates needed to determine microtubule depolymerization rates with high accuracy (Experimental Procedures, supplemental Movie 3). These measurements revealed that α1A/βIII microtubules depolymerize slower than brain microtubules (30.5 ± 1.3 μm/min versus 39.9 ± 1.5 μm/min; Fig. 4D). This suggests that microtubules with different chemical compositions (isoform or posttranslational modifications) have the potential to generate different end depolymerization forces that could be harnessed to move cargo in the cell, such as chromosomes during cell division (49).

The catastrophe (the transition between growth and shrinkage) frequency of recombinant microtubules is slightly reduced by 20% and 44% at the plus and minus-ends, respectively when compared with heterogenous brain tubulin (Figs. 4E and F). Interestingly, while 46% of brain microtubule exhibit growth at their minus ends, fewer than 7% of recombinant microtubules display minus-end dynamics under our assay conditions. Early studies reported faster polymerization rates for αβIII tubulin (α denotes here an unknown mixture of α-tubulin isoforms) immunopurified from brain tubulin preparations than for brain tubulin (15). Those studies also found that αβIII tubulin immunopurified from brain tubulin preparations had higher dynamicity than brain tubulin, while our measurements with recombinant α1A/βIII show lower dynamicity for this species than for brain microtubules (1.31 ± 0.05 μm/min *versus* 2.30 ± 0.07 μm/min for α1A/βIII and brain, respectively; Experimental Procedures). However, it is important to note that the tubulin used in these earlier studies had an unknown α-tubulin composition and a poorly defined mixture of diverse posttranslational modifications, unlike our recombinant tubulin, which contains a single α and β-tubulin isoform and is unmodified (Fig. 1A and Experimental Procedures). It is unclear at this point whether the subtle differences in dynamics we observe between the recombinant α1A/βIII microtubules and heterogenous mosaic brain microtubules are due to isoform differences, purification method and/or the abundant and diverse posttranslational modifications found on brain microtubules. Future studies with recombinantly expressed isoforms and quantitatively defined postranslationally modified tubulin using the expression and purification system described here will shed light on their individual contributions to dynamic instability parameters.

DISCUSSION

Using our dual-tag purification system for recombinant tubulin we report for the first time the structure and *in vitro* dynamics parameters for isotypically pure human unmodified microtubules, an essential and important first step in quantitatively establishing the correlates between sequence and dynamics for mammalian microtubules. The dual tag selection system is necessary as a single tag purification strategy results in significant levels of contamination with endogenous tubulin (~30% of insect α-tubulin if α-tubulin is not selected *via* affinity tag purification). Thus, our tagging and purification strategy allows the characterization of both α- and β-tubulin engineered constructs. The majority of *in vitro* dynamics studies presently performed use heterogenous mosaic brain microtubules with isoform composition and posttranslational modifications different from those found *in vivo*, for example in an epithelial cell or the axonal or dendritic compartment of a neuron. A recent study revealed different activities of the *S. cerevisiae* Stu2p on yeast microtubules compared to heterogeneous brain microtubules (50), indicating the importance of examining the effects of regulators with the physiologically relevant tubulin substrate. Our study establishes a system to examine the dynamics of mammalian microtubules with well-defined tubulin species and opens the way to study tubulin isoform-specific effects of microtubule associated proteins and motors and uncover the tubulin sequence elements critical for their recruitment and activation.

ACCESSION NUMBERS

The PDB and EMDB accession codes for the GMPCPP α1A/βIII microtubule reconstruction are 5JCO and 8150, respectively.

ACKNOWLEDGEMENTS

J.A. and C.A.M. are supported by the Medical Research Council, UK. A.V., J.O.S., A.S. and A.R.-M. are supported by the Intramural Programs of the National Institute of Neurological Disorders and Stroke (NINDS) and the National Heart, Lung and Blood Institute (NHLBI), NIH.

AUTHOR CONTRIBUTIONS

A.R-M. conceived project, A.V and J.O.S. performed and analyzed dynamics assays, J.A. determined EM structure, A.S. purified recombinant tubulin. All authors interpreted data. A.R.-M. wrote manuscript with contributions from A.V., J.O.S., J.A. and C.A.M.

References

1. Mitchison, T., and Kirschner, M. (1984) Dynamic instability of microtubule growth. *Nature* **312**, 237-242
2. Bieling, P., Laan, L., Schek, H., Munteanu, E. L., Sandblad, L., Dogterom, M., Brunner, D., and Surrey, T. (2007) Reconstitution of a microtubule plus-end tracking system in vitro. *Nature* **450**, 1100-1105
3. Brouhard, G. J., Stear, J. H., Noetzel, T. L., Al-Bassam, J., Kinoshita, K., Harrison, S. C., Howard, J., and Hyman, A. A. (2008) XMAP215 is a processive microtubule polymerase. *Cell* **132**, 79-88
4. Leandro‐García, L. J., Leskelä, S., Landa, I., Montero‐Conde, C., López‐Jiménez, E., Letón, R., Cascón, A., Robledo, M., and Rodríguez‐Antona, C. (2010) Tumoral and tissue‐specific expression of the major human β‐tubulin isotypes. *Cytoskeleton* **67**, 214-223
5. Miller, K. E., and Joshi, H. C. (1996) Tubulin transport in neurons. *J. Cell Biol.* **133**, 1355-1366
6. Yu, I., Garnham, C. P., and Roll-Mecak, A. (2015) Writing and reading the tubulin code. *J. Biol. Chem* **290**, 17163-17172
7. Verhey, K. J., and Gaertig, J. (2007) The tubulin code. *Cell Cycle* **6**, 2152-2160
8. Weisenberg, R. C. (1972) Microtubule formation in vitro in solutions containing low calcium concentrations. *Science* **177**, 1104-1105
9. Sullivan, K. F., and Cleveland, D. W. (1986) Identification of conserved isotype-defining variable region sequences for four vertebrate beta tubulin polypeptide classes. *Proc. Natl. Acad. Sci. U.S.A.* **83**, 4327-4331
10. Banerjee, A., Roach, M., Wall, K., Lopata, M., Cleveland, D., and Luduena, R. (1988) A monoclonal antibody against the type II isotype of beta-tubulin. Preparation of isotypically altered tubulin. *J. Biol. Chem* **263**, 3029-3034
11. Garnham, C. P., and Roll‐Mecak, A. (2012) The chemical complexity of cellular microtubules: Tubulin post‐translational modification enzymes and their roles in tuning microtubule functions. *Cytoskeleton* **69**, 442-463
12. Zambito, A. M., Knipling, L., and Wolff, J. (2002) Charge variants of tubulin, tubulin S, membrane-bound and palmitoylated tubulin from brain and pheochromocytoma cells. *BBA- Proteins Proteom.* **1601**, 200-207
13. Trinczek, B., Marx, A., Mandelkow, E. M., Murphy, D. B., and Mandelkow, E. (1993) Dynamics of microtubules from erythrocyte marginal bands. *Mol. Biol. Cell* **4**, 323-335
14. Newton, C. N., DeLuca, J. G., Himes, R. H., Miller, H. P., Jordan, M. A., and Wilson, L. (2002) Intrinsically slow dynamic instability of HeLa cell microtubules in vitro. *J. Biol. Chem* **277**, 42456-42462
15. Panda, D., Miller, H. P., Banergee, A., Ludena, R. F., and Wilson, L. (1994) Microtubule dynamics in vitro are regulated by the tubulin isotype composition. *Proc Natl Acad Sci* **91**, 11358-11362
16. Minoura, I., Hachikubo, Y., Yamakita, Y., Takazaki, H., Ayukawa, R., Uchimura, S., and Muto, E. (2013) Overexpression, purification, and functional analysis of recombinant human tubulin dimer. *FEBS Lett.* **587**, 3450-3455
17. Valenstein, M., and Roll-Mecak, A. (2016) Graded Control of Microtubule Severing by Tubulin Glutamylation. *Cell*, 911-921
18. Sirajuddin, M., Rice, L. M. & Vale, R. D. . (2014) Regulation of microtubule motors by tubulin isotypes and post-translational modifications. *Nat Cell Bio* **16**, 335-344

19. Atherton, J., Farabella, I., Yu, I. M., Rosenfeld, S. S., Houdusse, A., Topf, M., and Moores, C. A. (2014) Conserved mechanisms of microtubule-stimulated ADP release, ATP binding, and force generation in transport kinesins. *Elife* **3**, e03680
20. Kremer, J. R., Mastronarde, D. N., and McIntosh, J. R. (1996) Computer visualization of three-dimensional image data using IMOD. *J. Struct. Biol.* **116**, 71-76
21. Abrishami, V., Vargas, J., Li, X., Cheng, Y., Marabini, R., Sorzano, C. Ó. S., and Carazo, J. M. (2015) Alignment of direct detection device micrographs using a robust Optical Flow approach. *J. Struct. Biol.* **189**, 163-176
22. de la Rosa-Trevín, J., Otón, J., Marabini, R., Zaldívar, A., Vargas, J., Carazo, J., and Sorzano, C. (2013) Xmipp 3.0: an improved software suite for image processing in electron microscopy. *J. Struct. Biol.* **184**, 321-328
23. Mindell, J. A., and Grigorieff, N. (2003) Accurate determination of local defocus and specimen tilt in electron microscopy. *J. Struct. Biol.* **142**, 334-347
24. Ludtke, S. J., Baldwin, P. R., and Chiu, W. (1999) EMAN: semiautomated software for high-resolution single-particle reconstructions. *J. Struct. Biol.* **128**, 82-97
25. Sindelar, C. V., and Downing, K. H. (2007) The beginning of kinesin's force-generating cycle visualized at 9-A resolution. *J. Cell Biol.* **177**, 377-385
26. Chen, S., McMullan, G., Faruqi, A. R., Murshudov, G. N., Short, J. M., Scheres, S. H., and Henderson, R. (2013) High-resolution noise substitution to measure overfitting and validate resolution in 3D structure determination by single particle electron cryomicroscopy. *Ultramicroscopy* **135**, 24-35
27. Emsley, P., Lohkamp, B., Scott, W. G., and Cowtan, K. (2010) Features and development of Coot. *Acta Crystallogr. D.* **66**, 486-501
28. Zhang, R., Alushin, G. M., Brown, A., and Nogales, E. (2015) Mechanistic Origin of Microtubule Dynamic Instability and Its Modulation by EB Proteins. *Cell* **162**, 849-859
29. Brown, A., Long, F., Nicholls, R. A., Toots, J., Emsley, P., and Murshudov, G. (2015) Tools for macromolecular model building and refinement into electron cryo-microscopy reconstructions. *Acta Crystallogr D Biol Crystallogr* **71**, 136-153
30. Pecqueur, L., Duellberg, C., Dreier, B., Jiang, Q., Wang, C., Plückthun, A., Surrey, T., Gigant, B., and Knossow, M. (2012) A designed ankyrin repeat protein selected to bind to tubulin caps the microtubule plus end. *Proc. Natl. Acad. Sci. U.S.A.* **109**, 12011-12016
31. Nicholls, R. A., Long, F., and Murshudov, G. N. (2012) Low-resolution refinement tools in REFMAC5. *Acta Crystallogr. D.* **68**, 404-417
32. Gell, C., Bormuth, V., Brouhard, G., Cohen, D., S, D., Friel, C., Helenius, J., Nitzsche, B., Petzold, H., Ribbe, J., Schaffer, E., Stear, J., Trushko, A., Varga, V., Widlund, P., Zanic, M., and Howard, J. (2010) Microtubule dynamics reconstituted *in vitro* and image by single-molecule fluorescence microscopy. *Methods Cell Biol.* **95**, 221-245
33. Szyk, A., Deaconescu, A. M., Spector, J., Goodman, B., Valenstein, M. L., Ziolkowska, N. E., Kormendi, V., Grigorieff, N., and Roll-Mecak, A. (2014) Molecular basis for age-dependent microtubule acetylation by tubulin acetyltransferase. *Cell* **157**, 1405-1415
34. Ziółkowska, N. E., and Roll-Mecak, A. (2013) In vitro microtubule severing assays. in *Adhesion Protein Protocols*, Springer. pp 323-334
35. Toso, R. J., Jordan, M. A., Farrell, K. W., Matsumoto, B., and Wilson, L. (1993) Kinetic stabilization of microtubule dynamic instability in vitro by vinblastine. *Biochemistry* **32**, 1285-1293
36. Burgoyne, R. D., Cambray-Deakin, M. A., Lewis, S. A., Sarkar, S., and Cowan, N. J. (1988) Differential distribution of beta-tubulin isotypes in cerebellum. *EMBO J.* **7**, 2311
37. Kavallaris, M. (2010) Microtubules and resistance to tubulin-binding agents. *Nat. Rev. Cancer* **10**, 194-204
38. Peris, L., Thery, M., Fauré, J., Saoudi, Y., Lafanechère, L., Chilton, J. K., Gordon-Weeks, P., Galjart, N., Bornens, M., and Wordeman, L. (2006) Tubulin tyrosination is a

major factor affecting the recruitment of CAP-Gly proteins at microtubule plus ends. *J. Cell Biol.* **174**, 839-849
39. Peris, L., Wagenbach, M., Lafanechère, L., Brocard, J., Moore, A. T., Kozielski, F., Job, D., Wordeman, L., and Andrieux, A. (2009) Motor-dependent microtubule disassembly driven by tubulin tyrosination. *J. Cell Biol.* **185**, 1159-1166
40. Vale, R. D., Coppin, C. M., Malik, F., Kull, F. J., and Milligan, R. A. (1994) Tubulin GTP hydrolysis influences the structure, mechanical properties, and kinesin-driven transport of microtubules. *J. Biol. Chem* **269**, 23769-23775
41. Nogales, E., Wolf, S. G., and Downing, K. H. (1998) Structure of the αβ tubulin dimer by electron crystallography. *Nature* **391**, 199-203
42. Garnham, C. P., Vemu, A., Wilson-Kubalek, E. M., Yu, I., Szyk, A., Lander, G. C., Milligan, R. A., and Roll-Mecak, A. (2015) Multivalent Microtubule Recognition by Tubulin Tyrosine Ligase-like Family Glutamylases. *Cell* **161**, 1112-1123
43. Roll-Mecak, A. (2015) Intrinsically disordered tubulin tails: complex tuners of microtubule functions? in *Semin Cell Dev Biol*, Elsevier
44. Alushin, G. M., Ramey, V. H., Pasqualato, S., Ball, D. A., Grigorieff, N., Musacchio, A., and Nogales, E. (2010) The Ndc80 kinetochore complex forms oligomeric arrays along microtubules. *Nature* **467**, 805-810
45. Alushin, G. M., Lander, G. C., Kellogg, E. H., Zhang, R., Baker, D., and Nogales, E. (2014) High-resolution microtubule structures reveal the structural transitions in αβ-tubulin upon GTP hydrolysis. *Cell* **157**, 1117-1129
46. Horio, T. H., H. . (1986) Visualization of the dynamic instability of individual microtubules by dark-field microscopy. *Nature* **321**, 605-607
47. Mandelkow, E. M., Mandelkow, E., and Milligan, R. A. (1991) Microtubule dynamics and microtubule caps: a time-resolved cryo-electron microscopy study. *J. Cell Biol.* **114**, 977-991
48. Gardner, M. K., Charlebois, B. D., Jánosi, I. M., Howard, J., Hunt, A. J., and Odde, D. J. (2011) Rapid microtubule self-assembly kinetics. *Cell* **146**, 582-592
49. Grishchuk, E. L., Molodtsov, M. I., Ataullakhanov, F. I., and McIntosh, J. R. (2005) Force production by disassembling microtubules. *Nature* **438**, 384-388
50. Podolski, M., Mahamdeh, M., and Howard, J. (2014) Stu2, the budding yeast XMAP215/Dis1 homolog, promotes assembly of yeast microtubules by increasing growth rate and decreasing catastrophe frequency. *J. Biol. Chem* **289**, 28087-28093
51. Davis, I. W., Leaver-Fay, A., Chen, V. B., Block, J. N., Kapral, G. J., Wang, X., Murray, L. W., Arendall, W. B., 3rd, Snoeyink, J., Richardson, J. S., and Richardson, D. C. (2007) MolProbity: all-atom contacts and structure validation for proteins and nucleic acids. *Nucleic Acids Res* **35**, W375-383
52. Cardone, G., Heymann, J. B., and Steven, A. C. (2013) One number does not fit all: mapping local variations in resolution in cryo-EM reconstructions. *J. Struct. Biol.* **184**, 226-236
53. Sousa, D., and Grigorieff, N. (2007) Ab initio resolution measurement for single particle structures. *J. Struct. Biol.* **157**, 201-210

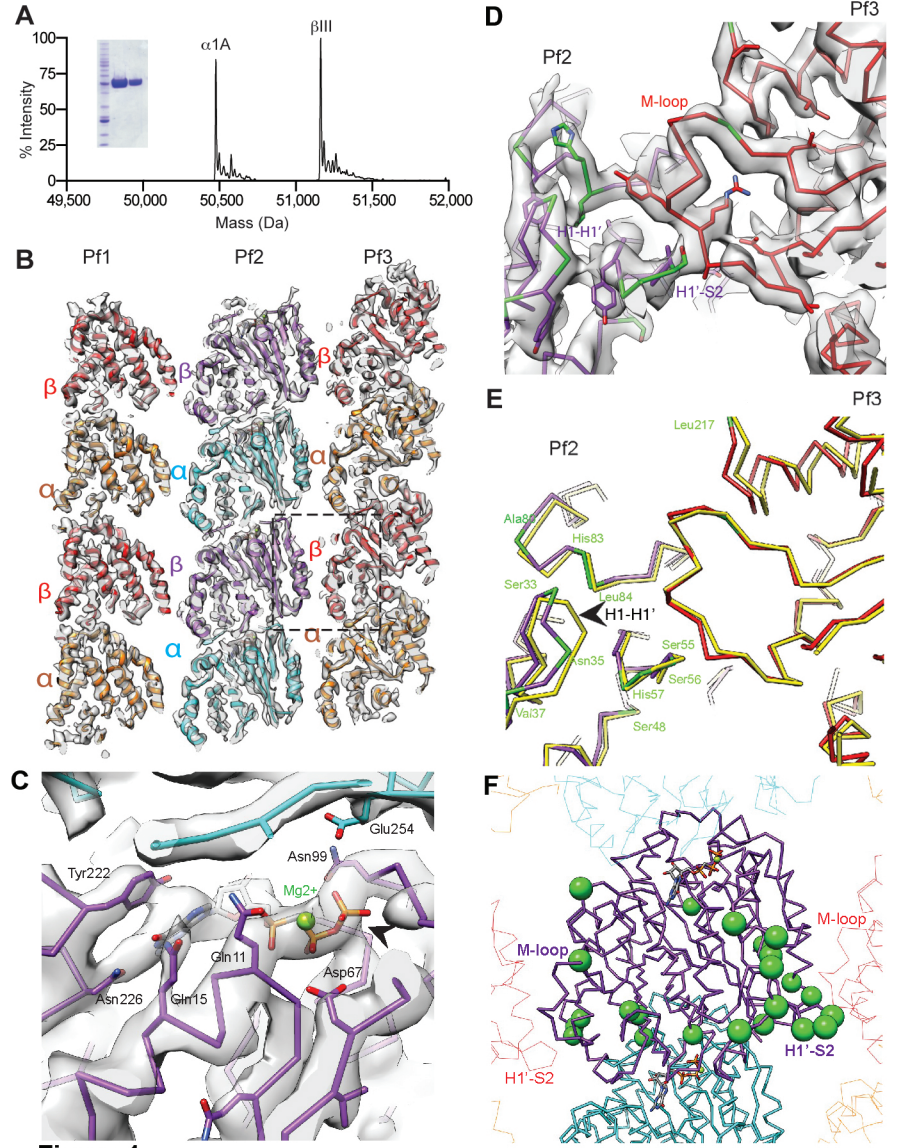
A
100
75
50
25
0
% Intensity
α1A
βIII
49,500
50,000
50,500
51,000
51,500
52,000
Mass (Da)
B
Pf1
Pf2
Pf3
β
α
C
Glu254
Asn99
Tyr222
Mg2+
Gln11
Asp67
Asn226
Gln15
D
Pf3
Pf2
M-loop
H1-H1'
H1'-S2
E
Pf3
Pf2
Leu217
Ala81
His83
Ser33
Leu84
H1-H1'
Ser55
Asn35
Ser56
His57
Val37
Ser48
F
M-loop
M-loop
H1'-S2
H1'-S2

Figure 1

FIGURE LEGENDS

FIGURE 1. Structure of unmodified single-isoform human α1A/βIII microtubules
A, Mass spectra and SDS-PAGE gel (inset) of recombinant human α1A/βIII tubulin purified to >99% homogeneity. The experimentally determined masses for α1A and βIII tubulin were 50,477.8 Da and 51,163.6 Da, respectively. The theoretical masses for α1A and βIII tubulin are 50,476.8 Da and 51,162.4 Da, respectively. B, Cryo-EM map (4.2Å resolution, 2.8 σ contour) and model of GMPCPP recombinant human α1A/βIII microtubules viewed from the lumen (three protofilaments shown). A central protofilament (Pf2) makes lateral contacts with adjacent protofilaments (Pf1 and Pf3); α-tubulin, orange, β-tubulin, red (Pf1, Pf3); α-tubulin, cyan; β-tubulin, purple (Pf2). C, The E-site in βIII-tubulin shows clear density for GMPCPP and its 3 phosphate groups. D, Model and map of the βIII-tubulin lateral interface (boxed and colored as in B). βIII-specific residues are in green. E, Superposition of the α1A/βIII (colored as in B) and brain (PDB: 3JAT; atomistic models of brain microtubules use the βII isotype sequence because it constitutes ~50% of these preparations (28,44); yellow) microtubule structures; residues specific to βIII are in green. F, βIII sequence variability concentrates at the lateral interface. Green spheres denote residues that are different between the βIII and βII isotypes, the most abundant tubulin isoforms in brain tubulin preparations (10).

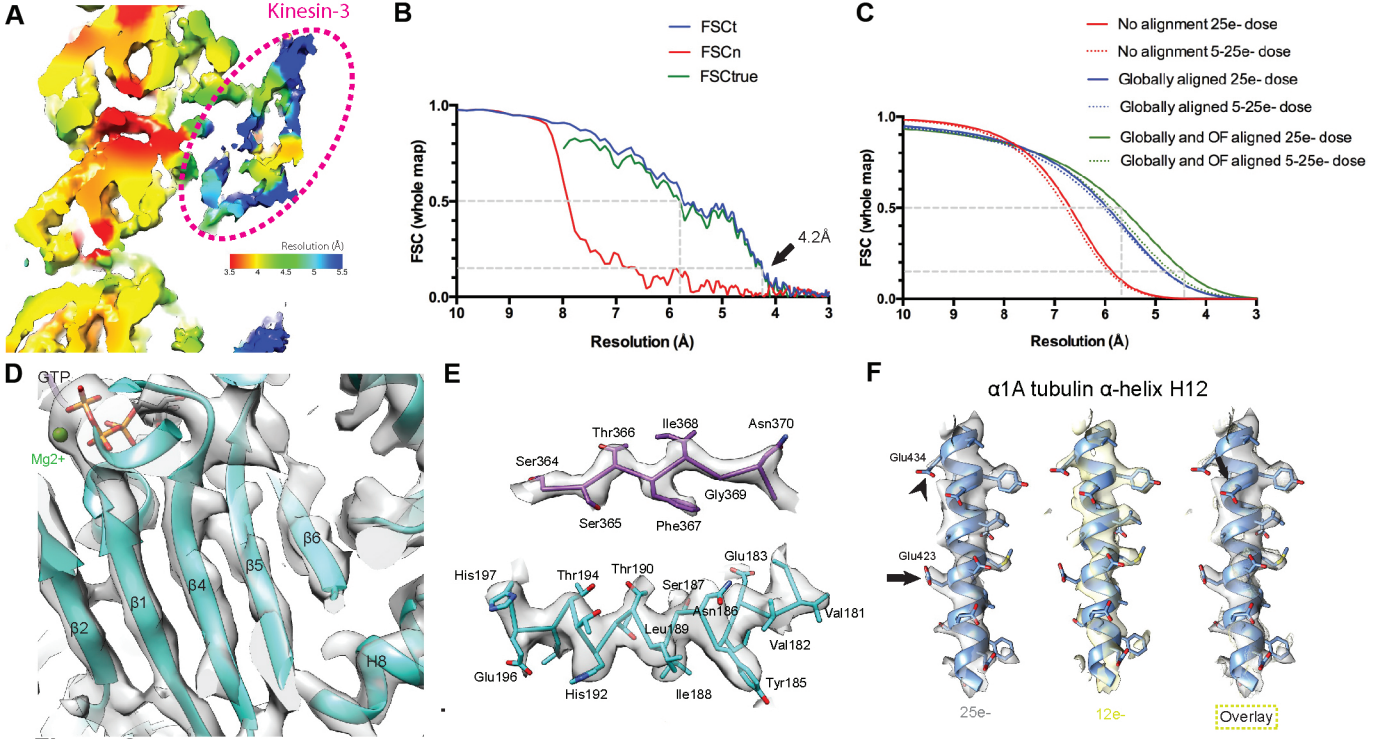
A
Kinesin-3
Resolution (Å)
3.5
4
4.5
5
5.5
B
FSCt
FSCn
FSCtrue
FSC (whole map)
1.0
0.5
0.0
10
9
8
7
6
5
4
3
Resolution (Å)
4.2Å
C
No alignment 25e- dose
No alignment 5-25e- dose
Globally aligned 25e- dose
Globally aligned 5-25e- dose
Globally and OF aligned 25e- dose
Globally and OF aligned 5-25e- dose
FSC (whole map)
Resolution (Å)
D
GTP
Mg2+
β1
β2
β4
β5
β6
H8
E
Thr366
Ile368
Asn370
Ser364
Gly369
Ser365
Phe367
His197
Thr194
Thr190
Glu183
Ser187
Asn186
Val181
Leu189
Val182
Glu196
His192
Ile188
Tyr185
F
α1A tubulin α-helix H12
Glu434
Glu423
25e-
12e-
Overlay

Figure 2

FIGURE 2. Data processing, map quality and resolution determination for cryo-EM reconstruction of recombinant human α1A/βIII microtubules

A, Local resolution estimates calculated using the Bsoft program blocres (52) were used to color the unfiltered whole reconstruction density. Red density corresponds to 3.5Å resolution, with a continuum of colors indicating the resolution gradient, ending with blue at 5.5Å resolution. Tubulin is at a higher resolution, ranging from ~3.5Å in central regions to ~ 4.5Å in more flexible peripheral surface exposed region. While used for the initial alignment, Kinesin-3 is less ordered (resolution of ~ 5.5Å) and excluded from display items. B, Fourier shell correlation (FSC) curves. The gold-standard noise-substitution test (26) on the whole microtubule+kinesin-3 map indicates no over-fitting at high resolution and an overall resolution of 4.2Å (FSCtrue at 0.143 cutoff). C, $R_{measure}$ (53) fitted curves give the same resolution estimate. Global alignment of whole movie frames improved resolution dramatically, while local alignment using an optical flow technique (21) yielded further improvements, especially for frames from early dosing of the data most susceptible to beam-induced motion. D, The higher resolution (< 4Å) in the tubulin dimer core is supported by clear density for the backbone and most side chains (see also panel E). E, Representative density for a β-strand in β-tubulin (top) and an α-helix in α-tubulin (bottom). F, Reconstructions from the first 12e- dose data (yellow) showed improved density for some side chains when compared with the 25e- dose data (grey), regardless of whether they were acidic. The highly negatively charged helix H12 of α-tubulin is shown. Arrowheads indicate acidic side chains that are notable for their different appearance in 12e- and 25e- maps.

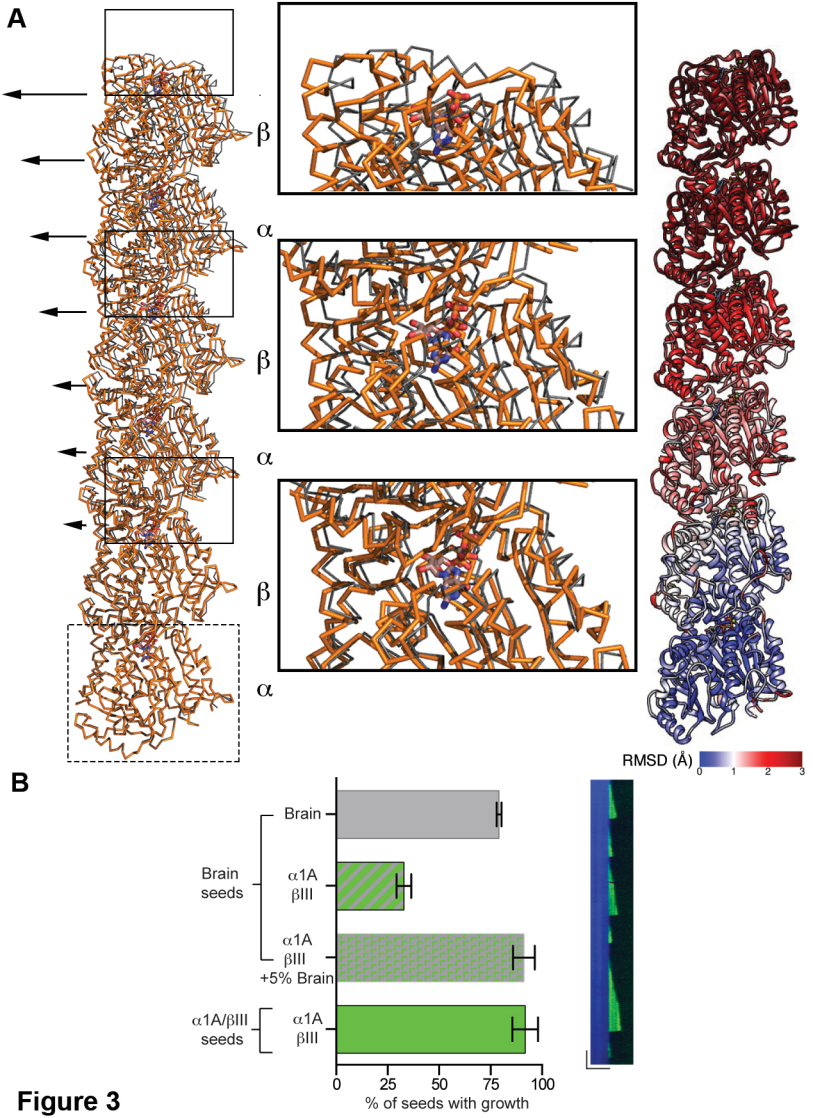
A
β
α
β
α
β
α
RMSD (Å)
0
1
2
3
B
Brain
Brain seeds
α1A βIII
α1A βIII +5% Brain
α1A/βIII seeds
α1A βIII
0
25
50
75
100
% of seeds with growth

Figure 3

FIGURE 3. Comparison between α1A/βIII and mosaic brain 14 protofilament microtubule structures

A, *Left panel,* Dimer displacement compared to the structure of mosaic brain microtubules PDB: 3JAT(28) as viewed from the microtubule lumen. The boxed α1A-tubulin protomer from the α1A/βIII structure (orange Cα trace) was superimposed on the α-tubulin protomer from the brain microtubule structure (grey Cα trace). Arrows indicate the gradual increase in displacement of the α1A/βIII heterodimers as one advances towards the plus-end of the protofilament. The GTP and GMPCPP in the N-site of α- and the E-site of β-tubulin are shown as ball-and-stick; *Middle panel,* Zoomed in view of regions highlighted by boxes in the left panel showing details of the displacement between the dimers from the recombinant α1A/βIII and brain microtubule structures; *Right panel,* Three α1A/βIII heterodimers within one protofilament colored according to main chain displacement from the brain microtubule structure. B, *Left panel,* Percentage of seeds that nucleate microtubules at 6μM tubulin. Brain, α1A/βIII, α1A/βIII + 5% brain tubulin elongated from brain seeds, α1A/βIII tubulin elongated from α1A/βIII seeds. More than 100 seeds across multiple chambers were counted for these measurements. *Right panel,* Kymograph of microtubule growth for recombinant α1A/βIII at 5.7 μM spiked with 5% Hilyte 488 brain tubulin (0.3μM) from brain GMPCPP seeds showing incorporation of the brain tubulin into the α1A/βIII lattice. Horizontal and vertical scale bar, 5 μm and 2 minutes, respectively.

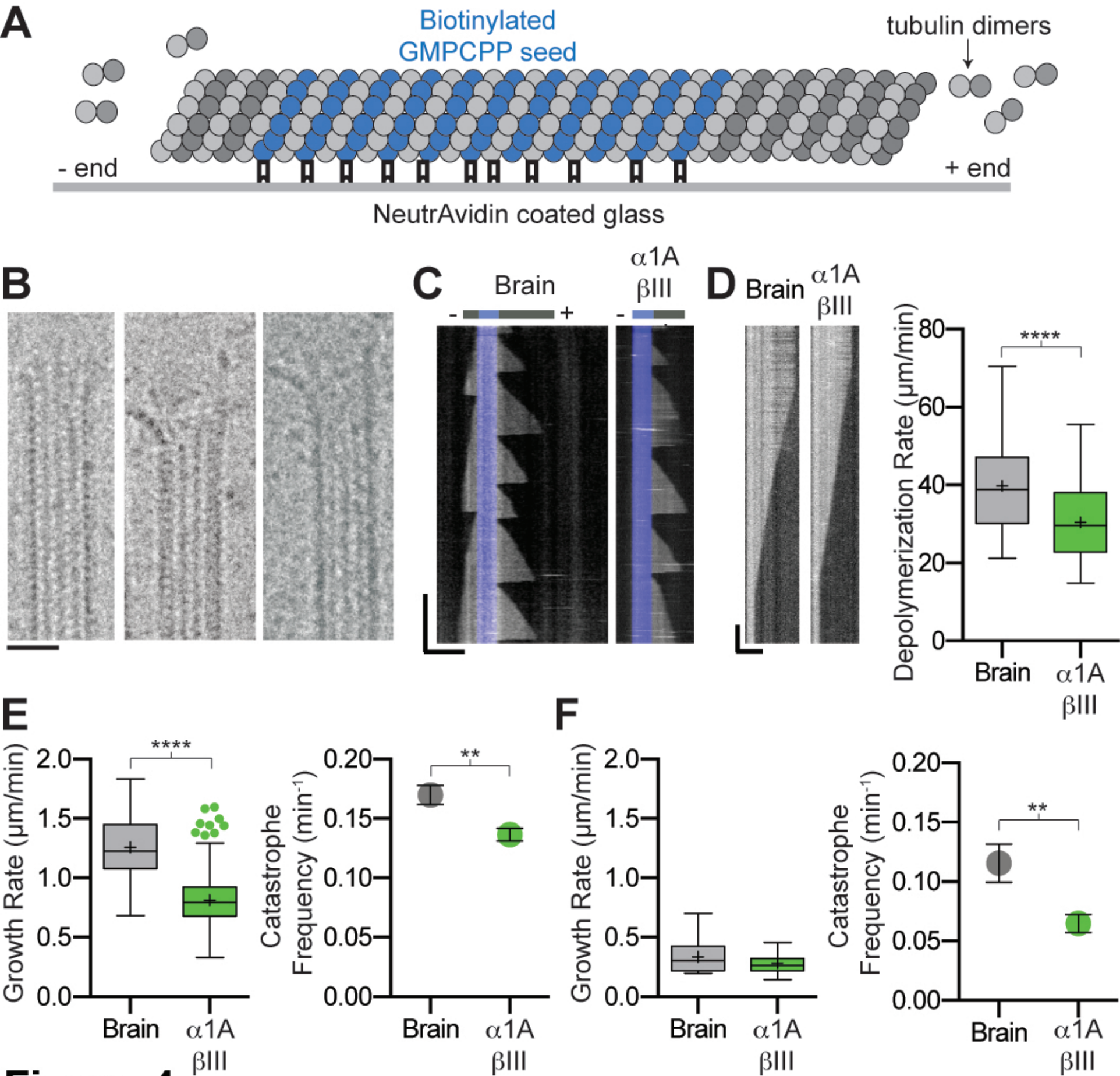
A
Biotinylated
GMPCPP seed
tubulin dimers
- end
+ end
NeutrAvidin coated glass
B
C
Brain
α1A
βIII
D
Brain
α1A
βIII
Depolymerization Rate (μm/min)
****
Brain
α1A
βIII
E
Growth Rate (μm/min)
****
Brain
α1A
βIII
Catastrophe
Frequency (min-1)
**
Brain
α1A
βIII
F
Growth Rate (μm/min)
Brain
α1A
βIII
Catastrophe
Frequency (min-1)
**
Brain
α1A
βIII

Figure 4

FIGURE 4. Dynamic parameters of recombinant human α1A/βIII microtubules
A, Schematic of assay design (Experimental Procedures). B, Micrographs of representative dynamic α1A/βIII microtubule ends. Scale bar, 20 nm. C, Kymographs showing typical microtubule growth for brain and recombinant α1A/βIII tubulin at 9 μM. Blue marks the GMPCPP seed. Horizontal and vertical scale bars, 5 μm and 5 minutes, respectively. D*, Left panel*, Kymographs showing a typical depolymerization event for brain and α1A/βIII microtubules. Horizontal and vertical scale bar, 5 μm and 2 seconds, respectively. *Right panel*, Tukey plot showing plus-end depolymerization rates at 9μM tubulin; n = 55 and 58 events for brain and α1A/βIII microtubules, respectively. E, Plus end dynamics of brain and α1A/βIII tubulin at 9 μM tubulin. *Left panel*, Tukey plot showing growth rates; n = 255 and 504 events for brain and α1A/βIII tubulin, respectively. *Right panel*, Catastrophe frequencies; n = 48 and 167 microtubules for brain and α1A/βIII tubulin, respectively. F, Minus end dynamics of brain and α1A/βIII tubulin at 9 μM tubulin. *Left panel*, Tukey plot showing growth rates; n = 32 and 25 events for brain and α1A/βIII tubulin, respectively. *Right panel*, Catastrophe frequencies; n = 7 and 16 microtubules for brain and α1A/βIII tubulin, respectively. Error bars represent s.e.m. ** and ****, *p* values <0.01 and < 0.0001, respectively determined by unpaired *t*-test.